Alexandria Journal of Mathematics (ISSN 2090-4320 )
Volume1 -Number2 - November 2010

# Two-Dimensional Fluid Flow Past a Rectangular Plate with Variable Initial Velocity

**S. B. Doma[1)], I. H. El-Sirafy[1)] and A. H. El-Sharif[2)]**

[1)]Faculty of Science, Alexandria University, Moharram Bey, Alexandria, Egypt.
E-mail address: sbdoma@sci.alex.edu.eg
[2)]Mathematics Department, Faculty of Science, Garyounis University, Benghazi, Libya.

**Abstract**
We have investigated the motion of the time-independent flow of a viscous incompressible fluid passing a rectangular plate. The cross-section of this plate is considered to be in the form of a rectangle with dimensions $2W$ transverse to the flow and $T$ along the flow. The fluid is assumed to be steady flow of water with incident velocity equals $V_0 e^{-x}$. The boundary conditions are discussed in details. The resulting equations are solved numerically. Accordingly, the values of the pressure force, the velocity magnitude, vorticity magnitude and the stream function are given and analyzed at each position point.
**Key Words**: Elliptic-partial differential equations, fluid flow, two-dimensional problems.

## 1. Introduction

The methods of solution of elliptic, hyperbolic and parabolic partial differential equations are very interesting in mathematical physics and engineering sciences. The boundary conditions imposed on such problems make the difference from problem to another and accordingly the branch of computational physics is considered now as an independent subject that attracts the mathematicians, physicists and engineers. Elliptic partial differential equations are of wide applications in fluid mechanics, engineering sciences and mathematical physics. In this paper we are interested in the applications of elliptic partial differential equations in fluid mechanics.

The two-dimensional flow of power-law fluids over an isolated unconfined square cylinder has been investigated numerically in [1,2] in the range of conditions $1 \leq R_e \leq 45$ and $0.5 \leq n \leq 2.0$. The global quantities such as wake length, drag coefficients and the detailed kinematic variables like stream function, vorticity and so on, have been calculated for the above range of conditions. In particular, the effects of Reynolds number and of the power-law index have been investigated in the steady flow regime. The shear-thinning fluid behavior increases the drag above its Newtonian value whereas the shear-thickening behavior reduces the drag below its Newtonian value. However, as the value of the Reynolds number is gradually increased, the role of power-law index diminishes. Similarly, the wake size is shorter in shear-thinning fluids than that in Newtonian fluids under otherwise identical conditions.

A numerical study on the uniform shear flow past a long cylinder of square cross-section placed parallel to a plane wall has been made in [3]. The cylinder is considered to be within the boundary layer of the wall. The maximum gap between the plane wall to the cylinder is taken to be 0.25 times the cylinder height. The authors investigated the flow when the regular vortex shedding from the cylinder is suppressed. The governing unsteady Navier-Stokes equations are discretized through the finite volume method on staggered grid system. A pressure correction based iterative algorithm, SIMPLER, has been used to compute the discretized equations

iteratively. The authors found that the critical value of the gap height for which vortex shedding is suppressed depends on the Reynolds number, which is based on the height of the cylinder and the incident stream at the surface of the cylinder. At high Reynolds number ($Re \geq 500$) however, a single row of negative vortices occurs for wall to cylinder gap height $L \geq 0.2$. The shear layer that emerges from the bottom face of the cylinder reattaches to the cylinder itself at this gap hight.

Hydrodynamic equations for ideal incompressible fluid are written in [4] in terms of generalized stream function. Two-dimensional version of these equations is transformed to the form of one dynamic equation for the stream function. This equation contains arbitrary function which is determined by inflow conditions given on the boundary. To determine unique solution, velocity and vorticity (but not only velocity itself) must be given on the boundary. This unexpected circumstance may be interpreted in the sense that the fluid has more degrees of freedom than it was believed. Besides, the vorticity is a less observable quantity as compared with the velocity. It is shown that the Clebsch potentials are used essentially at the description of vortical flow.

The authors in [5] considered the numerical simulation of the two-dimensional viscous flow over a solid ellipse with an aspect ratio equal 3.5. Sufficiently far from the ellipse, the flow is assured potential. The flow is modeled by the two dimensional partial differential equations of conservation of mass and moment, using elliptic coordinates. The finite volume method is used to discritize the model equations. The numerical solutions revealed that the flow over the ellipse is steady with zero vortex up to Re = 40. For Reynolds numbers between 50 and 190, the flow is steady with two vortices in the wake. For Re = 210 the flow becomes unstable with harmonic oscillations. The two vortices are alternate in the time with a Strouhal number equal to 0.2075. For the Reynolds number between 220 and 280 the vortices are detached one after other. The spectral analysis of the discrete time variation of the flow velocity at a point within the upper vortex shows that the dominant oscillations frequency is f = 0.2748.

The latest developments in the simulation of turbulence by detached eddy simulation (DES) have suggested that this technique might be able to replace large eddy simulation (LES) within the next decade [6]. The results of the flow past a square cylinder show that this approach is quite inexpensive compared to LES while capturing the most important features of the flow. The study in [6] extends the range of applications of DES towards a fully unsteady three-dimensional case with strong streamline curvature, which is known to be a major problem for Reynolds-averaged Navier–Stokes equation (RANS) methods. The case considered in [6] is the turbulent flow over wall-mounted cubes at a Reynolds number of $R_e = 1.3 \times 10^4$. The results demonstrate that DES is able to capture the most dominant flow patterns like LES, while RANS only gives only a poor representation of the unsteady flow phenomena.

The motion of a viscous incompressible fluid which is passing over a rectangular plate is thus an interesting research problem. Doma et al., investigated in [7] the motion of the time-independent flow of a viscous incompressible fluid passing a rectangular plate. The cross-section of this plate is considered to be in the form of a rectangle with dimensions $2W$ transverse to the flow and $T$ along the flow. The fluid is assumed to be steady flow of water with incident velocity equals $V_0$. The resulting equations are solved numerically. In the present paper we investigate the same problem investigated in [7] but with the difference that the initial velocity is considered now as a varying function in the form of $V_0 e^{-x}$. Accordingly, the values of the pressure force, the velocity magnitude, vorticity magnitude and the stream function are given and analyzed at each position point.

## 2. The Equations of Motion

The steady-state hydrodynamics in two dimensions, in our case, was considered for different Reynolds-number. The Reynolds-number $R_e$ in our case of incompressible fluid is defined as $R_e = \frac{V_0 h}{\nu}$, where $h$ is the step size dimension and $\nu$ is the kinematic viscosity. The magnitude of the initial velocity field was defined here by $V_0 e^{-x}$. Two fundamental equations are required for the mass density, $\rho$, and the velocity of the fluid element at each point in space, $\boldsymbol{V}$. The first of which is the continuity equation [8]

$$\frac{\partial \rho}{\partial t} + \nabla . \rho \boldsymbol{V} = 0, \tag{2.1}$$

and the second is the Navier-Stokes equation [5]

$$\frac{\partial \boldsymbol{V}}{\partial t} = -(\boldsymbol{V}.\nabla)\boldsymbol{V} - \frac{1}{\rho}\nabla P + \nu \nabla^2 \boldsymbol{V}, \tag{2.2}$$

where $P$ is the pressure and the kinematic viscosity $\nu$ is assumed constant. The first equation expresses the conservation of mass and the second equation expresses the conservation of momentum. We will assume that the temperature is constant throughout the fluid.

Furthermore, we will be interested in studying time-independent incompressible fluid flows, so that equations (2.1) and (2.2) can be rewritten in the following forms

$$\nabla . \boldsymbol{V} = 0, \tag{2.3}$$

$$(\boldsymbol{V}.\nabla)\boldsymbol{V} = -\frac{1}{\rho}\nabla P + \nu \nabla^2 \boldsymbol{V}. \tag{2.4}$$

For two-dimensional flow, these equations can be written explicitly in terms of the $x$ and $y$ components of the velocity field, denoted by $u$ and v, respectively:

$$\frac{\partial u}{\partial x} + \frac{\partial \mathrm{v}}{\partial y} = 0; \tag{2.5}$$

$$u\frac{\partial u}{\partial x} + \mathrm{v}\frac{\partial u}{\partial y} = -\frac{1}{\rho}\frac{\partial P}{\partial x} + \nu \nabla^2 u; \tag{2.6}$$

$$u\frac{\partial \mathrm{v}}{\partial x} + \mathrm{v}\frac{\partial \mathrm{v}}{\partial y} = -\frac{1}{\rho}\frac{\partial P}{\partial y} + \nu \nabla^2 \mathrm{v}. \tag{2.7}$$

The continuity equation (2.5) can be satisfied directly by introducing the stream function $\psi$, defined by [9]

$$u = \frac{\partial \psi}{\partial y}; \quad \mathrm{v} = -\frac{\partial \psi}{\partial x}, \tag{2.8}$$

such a $\psi$ function exists for all flows that satisfy the continuity equation. It can be seen also that $\boldsymbol{V}$ is tangent to contour lines of constant $\psi$, the stream lines. The vorticity is given by

$$\zeta = \frac{\partial \mathrm{u}}{\partial \mathrm{y}} - \frac{\partial \mathrm{v}}{\partial \mathrm{x}} = \nabla^2 \psi \tag{2.9}$$

It can also proved that

$$\nu \nabla^2 \zeta = \frac{\partial \psi}{\partial y}\frac{\partial \zeta}{\partial x} - \frac{\partial \psi}{\partial x}\frac{\partial \zeta}{\partial y} \tag{2.10}$$

Finally, the pressure can be given in terms of the stream function, as follows

$$\nabla^2 P = 2\rho\left\{\frac{\partial^2\psi}{\partial x^2}\frac{\partial^2\psi}{\partial y^2} - \left(\frac{\partial^2\psi}{\partial x\partial y}\right)^2\right\} \tag{2.11}$$

Equations (2.9), (2.10) and (2.11) are a set of non-linear elliptic equations, equivalent to the original equations (2.5), (2.6) and (2.7). This set by itself is an ill-posed problem, as some sort of boundary conditions is required [10]. These we will take to be of the Dirichlet type [6] for the stream function and the vorticity, and of the Neumann type [11] for the pressure. Accordingly, ψ is specified on some large closed curve in the $(x, y)$ plane (conveniently, the unit square). The boundary value problem is then to be used to find ψ everywhere.

For simplicity we will take the object to be translational invariant in one direction transverse to the flow, so that the fluid has a non-trivial motion only in two-coordinates $(x, y)$. This might describe a plate placed in a steady flow of water with incident velocity $V_0 e^{-x}$. We will also consider only the case where the cross-section of this plate is a rectangle with dimensions $2W$ transverse to the flow and $T$ along the flow. This will simplify the program needed to treat the boundary conditions, while still allowing the physics to be apparent. The problem is then analyzed and the resulting equations are solved, by writing a program in FORTRAN, to evaluate the stream function, the vorticity, the viscous force, and the pressure at each point on the unit square.

## 3. The Boundary Conditions

The boundary conditions on the centerline surfaces A and E of the plate are determined by symmetry. The $y-$ component of the velocity, v, must vanish on A and E, so that $\frac{\partial\psi}{\partial x}$ vanishes and accordingly A and E are stream lines. Moreover, since the normal velocity also vanishes on B, C, and D, the entire surface ABCDE is a single stream line. From symmetry, we can also conclude that the vorticity vanishes on A and E. The upstream surface F is contiguous with the smoothly flowing incident fluid, so that we can put

$$\mathrm{v} = -\frac{\partial\psi}{\partial x} = 0;\ \zeta = 0 \quad \text{on F.} \tag{3.1}$$

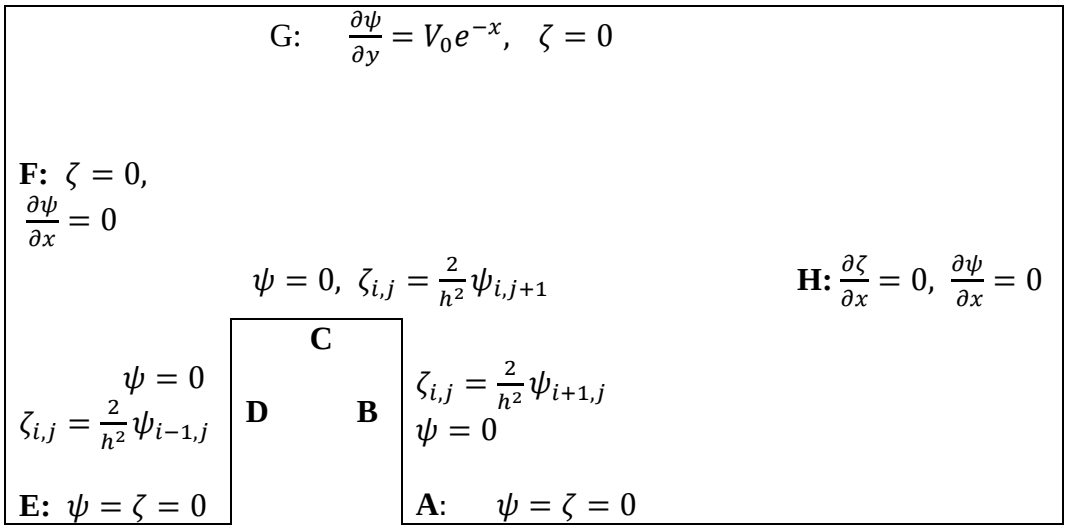


Fig. 1 Boundary conditions on $\psi$ and $\zeta$ for the flowing fluid and the obstacle for the upper part.

The boundary conditions on the upper boundary G are similarly straightforward. We may expect G to be in free flow, if the lattice is large enough. Hence,

$$u = \frac{\partial \psi}{\partial y} = V_0 e^{-x}; \ \zeta = 0 \quad \text{on G,} \tag{3.2}$$

are two appropriate choices.

The downstream boundary H is much more ambiguous and, so long as it is sufficiently far from the plate one convenient choice is

$$\frac{\partial \psi}{\partial x} = \frac{\partial \zeta}{\partial x} = 0 \qquad \text{on H.} \tag{3.3}$$

At the walls of the plates, (B, C, and D) one of the correct boundary conditions is that

$$\text{v} = -\frac{\partial \psi}{\partial x} = 0 \quad \text{on B, C, D.} \tag{3.4}$$

However, the other boundary condition appropriate for viscous flow is that the tangential velocity be zero,

$$u = \frac{\partial \psi}{\partial y} = 0 \quad \text{on B, C, D.} \tag{3.5}$$

The above boundary conditions are illustrated in Fig. (1).

The boundary conditions for the pressure on all surfaces are of the Neumann type, and follow from equations (2.6) and (2.7). From the symmetry, $\frac{\partial P}{\partial y} = 0$ on the centerlines A and E.

**4. Method of Solution**

To solve equations (2.9), (2.10) and (2.11) numerically we introduced, as in our previous paper [121], where the initial velocity is constant and equals $V_0$, a two-dimensional lattice of uniform spacing h having $N_x$ *and* $N_y$ points in the $x$ and $y$ directions, respectively, and use the indices $i$ and $j$ to measure these coordinates. It is convenient to scale the equations by measuring all lengths in units of $h$ and all velocities in units of $V_0$. The stream function is then measured in units of $V_0 h$, while the vorticity is in units of $\frac{V_0}{h}$, and the pressure is conveniently scaled by $\rho V_0^2$. The second step is to differencing equations (2.9), (2.10) and (2.11) by using symmetric second- and first-difference operators [12]. Accordingly, the lattice Reynolds number, $Re = \frac{V_0 h}{\nu}$, is a dimensionless measure of the strength of the viscous forces.

Our numerical method of solution of the resulting coupled non-linear elliptic partial differential equations for the stream function and the vorticity is by using the relaxation method iteratively [11]. In the model, a rectangular obstacle was defined with height $16h$ and width $8h$. Since, for simplicity, the incident fluid was in free flowing case parallel and far enough from the obstacle, the symmetry property was used. For solving the upper part of the flowing system in lattice space we take $N_x = 70$, $N_y = 24$, the vorticity relaxation $= 0.3$, and the stream relaxation $= 0.3$. Furthermore, the lattice Reynolds number was allowed to take on the values from 0.5 to 300. We begin the iteration scheme by choosing trial values corresponding to the free-flowing solution $\psi = y$ and $\zeta = 0$. We then perform one relaxation sweep of the first equation to get an improved value of $\psi$. For more details concerning the numerical method of solutions see [7].

## 5. Results and Conclusions

A computer program is written in FORTRAN to solve for $\psi, \zeta$, and $P$ subject to the boundary conditions discussed in section-3. The number of iterations required for the convergence of the solutions for different Reynolds numbers is shown in Table-1, together with the maximum and minimum values of the computed functions.

In Figs. 2-29 we present the variations of the static pressure, the velocity magnitude, the vorticity magnitude and the stream function, as functions of position, for $R_e = 0.5, 1, 10, 20, 100, 200$ and $300$, respectively.

Table-1 the number of iterations used for convergence of the solutions and their related minimum and maximum values for $v = V_0 e^{-x}$, decaying flow in the $x-$ direction.

| Reynolds number $R_e$ | Over-relaxation factor | Number of iterations | Stream function $\psi$ | | Vorticity magnitude $\zeta$ | | Static Pressure $P$ | | Velocity magnitude | |
|---|---|---|---|---|---|---|---|---|---|---|
| | | | Max | Min | Max | Min | Max | Min | Max | Min |
| 0.5 | 0.7 | 390 | 0.003 | 0 | 0.0025 | $1x10^{-7}$ | $7.3\,x10^{-6}$ | $-2\,x10^{-7}$ | $27.7\,x10^{-6}$ | 0 |
| 1.0 | 0.7 | 390 | 0.006 | 0 | 0.0056 | 0 | $15\,x10^{-6}$ | $-1\,x10^{-6}$ | $555\,x10^{-4}$ | 0 |
| 10 | 0.7 | 290 | 0.0613 | 0 | 0.1187 | $5x10^{-6}$ | $2.55\,x10^{-4}$ | $-135\,x10^{-6}$ | $5.52\,x10^{-4}$ | 0 |
| 20 | 0.7 | 260 | 0.1242 | 0 | 0.294 | $4x10^{-5}$ | $7.6\,x10^{-4}$ | $-6.4\,x10^{-4}$ | 0.00114 | 0 |
| 100 | 0.7 | 480 | 0.669 | 0 | 2.017 | $5.8x10^{-5}$ | 0.0156 | -14.9 e-3 | 0.00597 | 0 |
| 200 | 0.7 | 340 | 1.404 | 0 | 4.205 | $2.8x10^{-5}$ | 0.054 | -5.1 e-2 | 0.0119 | 0 |
| 300 | 0.2 | 9450 | 1.955 | 0 | 6.415 | $18.7x10^{-5}$ | 0.1912 | -0.062 | 0.0178 | 0 |

From the results we notice that for larger values of the Reynolds number, the pressure in front of the obstacle increases, knowing that when velocity increases the pressure is decreasing so that the pressure above the obstacle decreases when the velocity decreases.

The velocity magnitude will be increased with increasing the Reynolds number. Also, at high Reynolds numbers the position of high velocity of fluid is translated forward with the flow.

The convergence rates of the pressure function for different Reynolds number is seen in the figures.

The number of iterations used to approach the steady-state of the relaxation shows that, for larger value of the Reynolds number, the number of iterations for convergence of the stream function was slower than that for the vorticity function. The number of iterations for the vorticity function, indicates that the first consumed iterations for the vorticity function is reached and stayed within the convergence limit. The vorticity function was still refreshed differently for different iteration step because the dependence of the stream function was slower than that of the vorticity function. The convergence rates of the stream function and the vorticity function for different Reynolds number is shown in the figures.

The convergence rates in our previous paper [7], with initial velocity equals $V_0$, were found to be closed to that of our present situation, but the overall number of iterations is larger than that of the previous case in [7]. In general, for more strictly conditions such as in the present paper, the used iterations could be larger comparing to the previous case of [7]. Also, the same effects are obtained for greater value of Reynolds number.

The obtained results for Reynolds number $R_e = 1.0$ in the present paper, show that the number of iterations was, abnormally, lesser than that of the previous paper [7]. From Fig.-4, we notice, for the steady-state flowing system of Reynolds number $R_e = 1$ of vorticity near the

boundary, that the tail of the vorticity near the boundary H was distorted due to the new condition at H. This implied that the dimension in boundary A, was not sufficiently large enough. Therefore, by using the new condition at higher value of the Reynolds number, the dimensions of the artificial boundaries required to be larger and involved more computational consumption.

The low Reynolds number flowing system, for high value of viscosity, was actually a lubricant flow. For the Reynolds number $R_e = 0.5$ - case, according to Fig.-5 for the stream function contour, the flowing streamlines were smoothly overcome the obstacle and the shape was likely symmetric about the mid-axis but shifted to the right of the obstacle along the y-direction. Considering the plot of the vorticity, Fig.-4, the local maximum vortex were observed near the point-edge $(i = 10, j = 8)$ and $(i = 18, j = 8)$, and the rotational axes were found to be pointing out from the paper of the graph (z-direction). There were no curl enter (eddy current) observed behind the obstacle for Reynolds number $R_e = 0.5$ situation.

Comparing the vorticity contour plots for Reynolds number $R_e = 0.5, 1, and\ 10$, Figs.-4, -8, -12, respectively, the front section was found to be compressed and the tail was elongated as the Reynolds number increased. For the higher Reynolds number system, the greater distortion was observed. For the Reynolds number $R_e = 0.5$, the positive maximum value of the vertex at the point edge was shifted to the front one and the latter one disappeared or difficult to be observed.

However, there was a negative vortex, for Reynolds number $R_e = 0.5$, 1.0 and 10. The negative value of the vortex means that the curl exists but the rotation axis is anti-parallel to the z-direction (pointed into the paper) and the curl was eddy current.

According to the results of the velocity curves, Figures-3, -7 and -11, for Reynolds number $R_e = 0.5, 1.0\ and\ 10$, there were found center of the curl and are found to be behind to the obstacle.

The center of the eddy was found to be shifted to the right for larger Reynolds number, which was different from the vortex near the point edge of the obstacle. The eddy was found to be larger value (more negative) for larger Reynolds number.

For the classical fluid model, when there is a low density region created behind the obstacle, the fluid in the nearby region would be similar to the fluid into this low density region. The fluid flow into this region and the pattern was different for different Reynolds number systems. For low Reynolds number, it has large viscosity. This is possible for the lubricant flow, which is massive, such as for polymers or highly intermolecular force. The neighborhoods are highly effective to the flowing path, therefore the laminar flow is observed, for the high Reynolds number system (the larger value of the ratio of mass-diffusion time constant to mass-convection time constant). This implies that the jet existing through the divergent side and recirculation zones are easily appeared and the reversibility for the Reynolds number system is reduced. Therefore, for higher Reynolds number, the steady state solution is more difficultly to be approached due to the lowered reversibility. For high Reynolds number system, the used model will cause failure in the program.

**References**

[1] K. Dhiman, R. P. Chhabra and V. Eswaran, Steady Flow of Power-Law Fluids Across A Square Cylinder, Chemical Engineering Research and Design, **84**(A4): 300–310 (2006).

[2] A. K. Dhiman, R. P. Chabra and V. Eswaran, Steady Flow Across a Confined Square Cylinder: Effects of Power-Law Index and Blockage Ratio, J. Non-Newtonian Fluid Mech., (2008).
[3] S. Bhattacharyya, Kharagpur, and D. K. Maiti, Vortex shedding suppression for laminar flow past a square cylinder near a plane wall: a two-dimensional analysis, Acta Mechanica, **184**: 15–31 (2006).
[4] Yuri A. Rylov, Hydrodynamic Equations for Incompressible Inviscid Fluid In Terms of Generalized Stream Function, IJMMS, **11:** 541–570 (2004).
[5] M. Boubekri and M. Afrid, Some Modes of the Incompressible Flow on an Elliptic Cylinder at Low Reynolds Number, Journal of Engineering and Applied Sciences, **39**(1): 94-99 (2008).
[6] Stefan Schmidt, and Frank Thiele, Comparison of numerical methods applied to the flow over wall-mounted cubes, International Journal of Heat and Fluid Flow, **23:** 330–339 (2002).
[7] S. B. Doma, I. H. Elsirafy, M. M. El-Borai and A. H. El-Sharif, Two-Dimensional Fluid Flow Past A Rectangular Plate, International Journal of Applied Mathematics, 23(3): 367-387 (2010).
[8] L. D. Landau and E. M. Lifshitz, Fluid Mechanics, Pergamon Press, Singapore (1989).
[9] S. E. Koonin, Computational Physics, Addison-Wesley Publishing Company, Inc., New York (1886).
[10] B. Neat, Partial Differential Equations, MA 3132 Lectures Notes, Monterey, California 93943 (2002).
[11] H. Lomax and T. H. Pulliam, Fundamentals of Computation Dynamics, NASA Ames Research Center, August 26, (1999).
[12] E. Kreyszig, Advanced Engineering Mathematics, John Wiley and Sons, Inc., New York (2000).

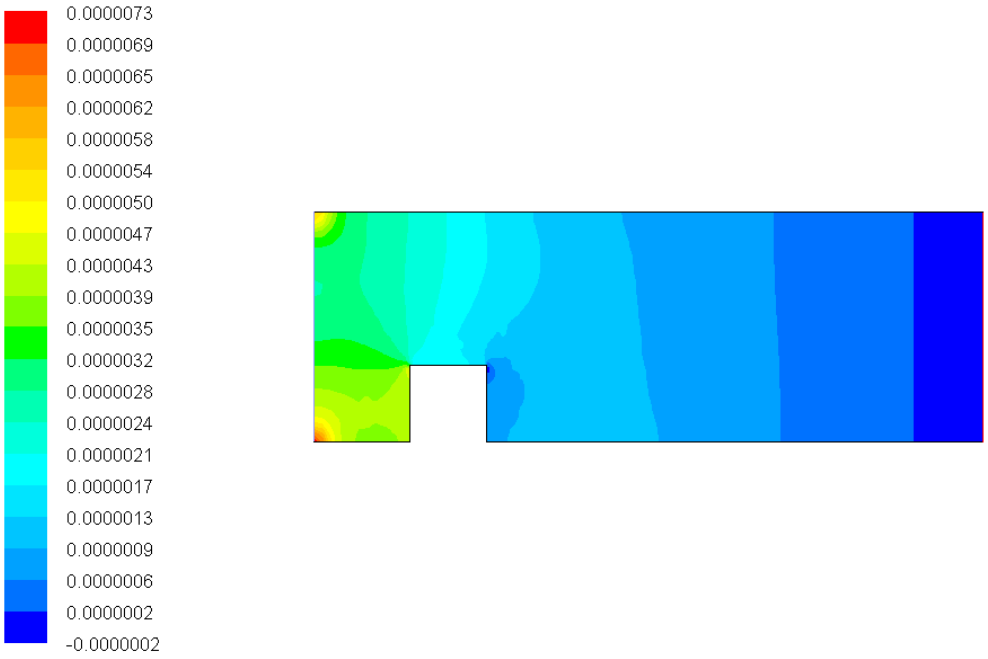


**Fig. 2 Static pressure ($R_e$= o.5)**

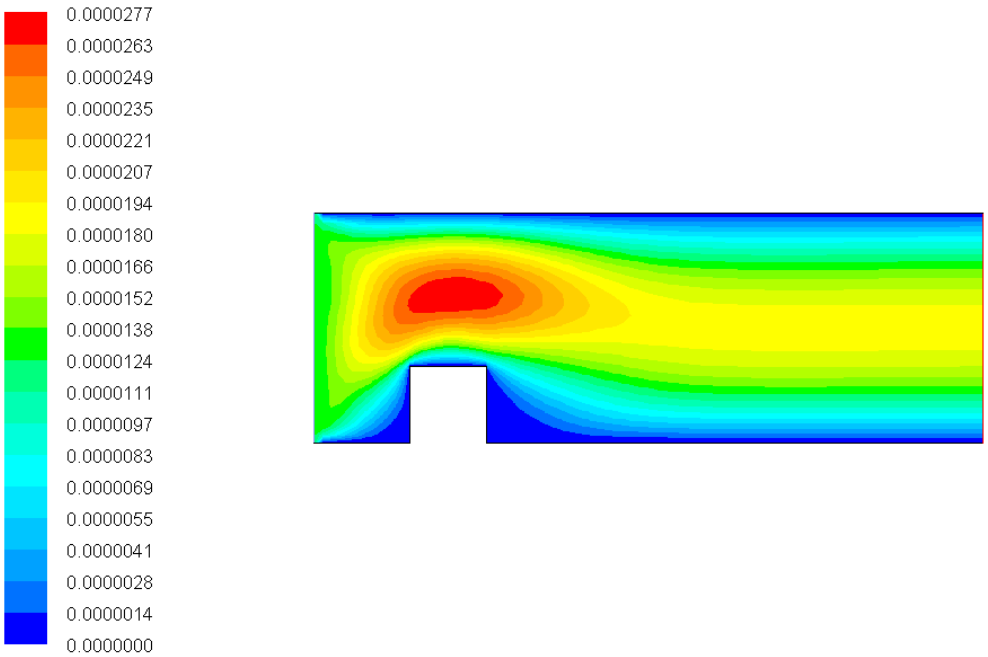


**Fig. 3 Velocity magnitude ($R_e$ = o.5)**

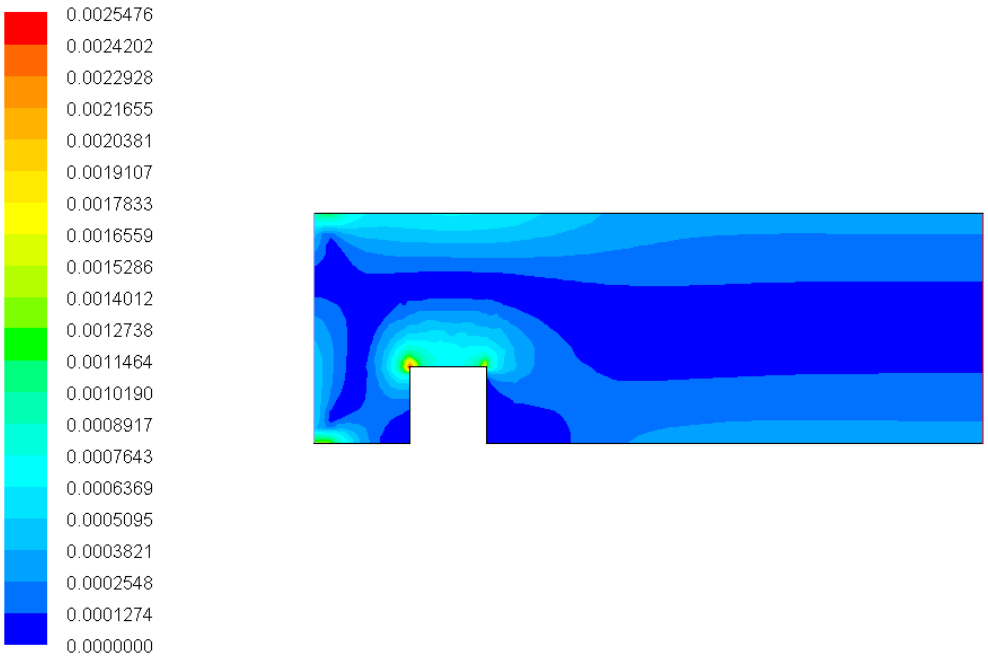


**Fig. 4 Vorticity magnitude (1/s) ($R_e$ = o.5)**

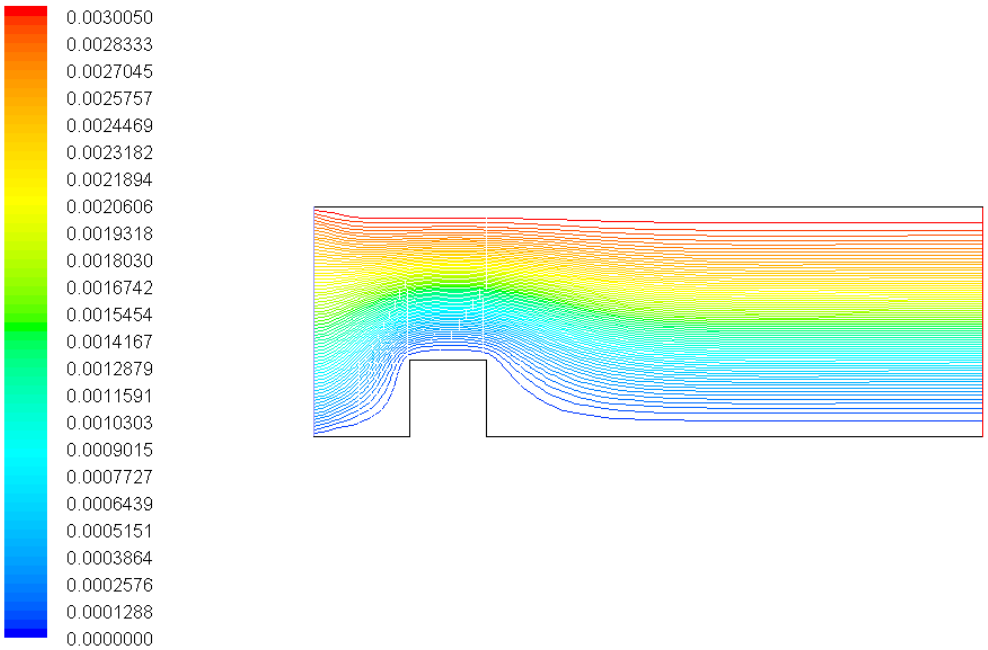


**Fig. 5 Stream function (Kg/s) ($R_e$= o.5)**

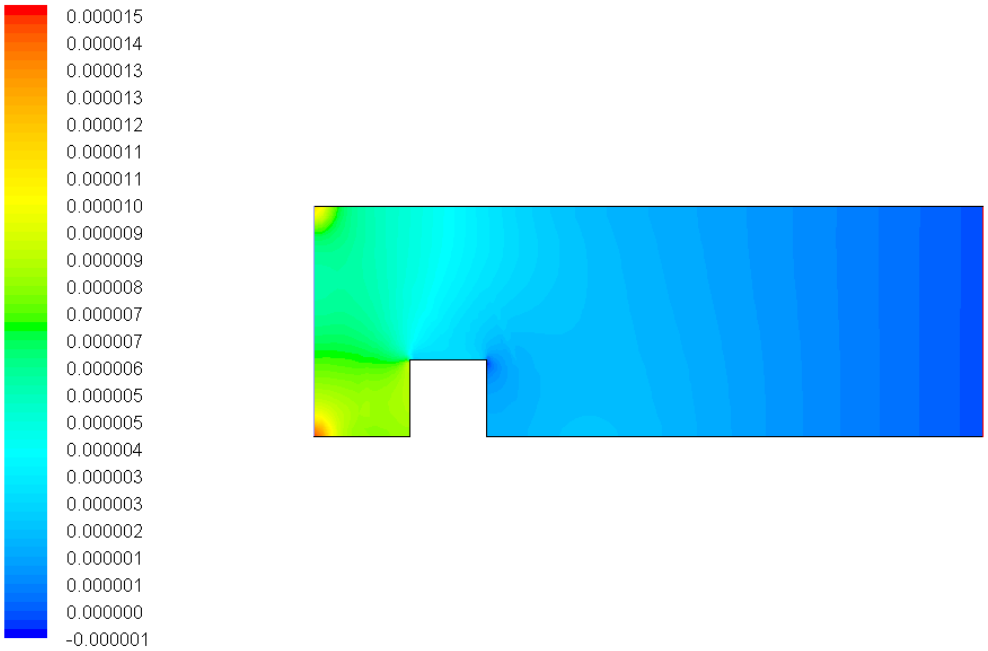


**Fig.6 Static pressure ($R_e$ = 1)**

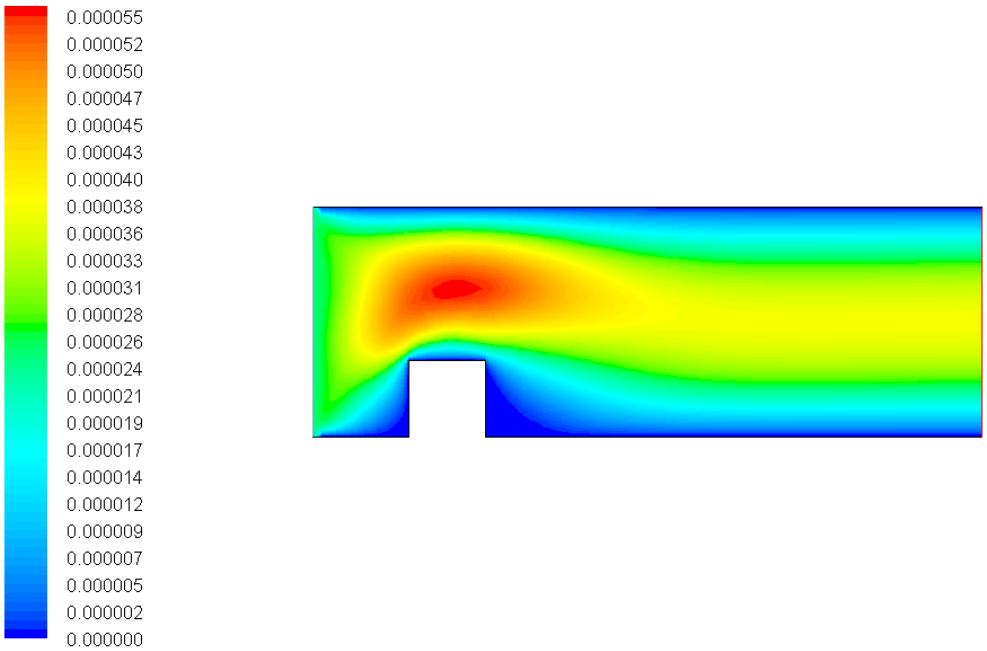


**Fig.7 Velocity ($R_e$ = 1)**

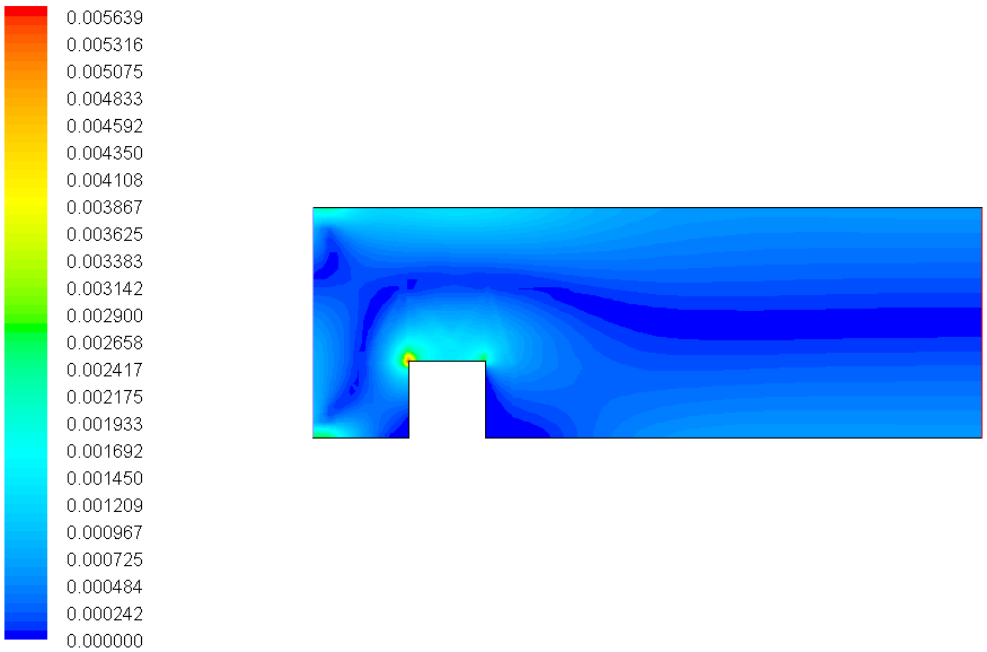


**Fig. 8 Vorticity magnitude (1/s) ($R_e$ = 1)**

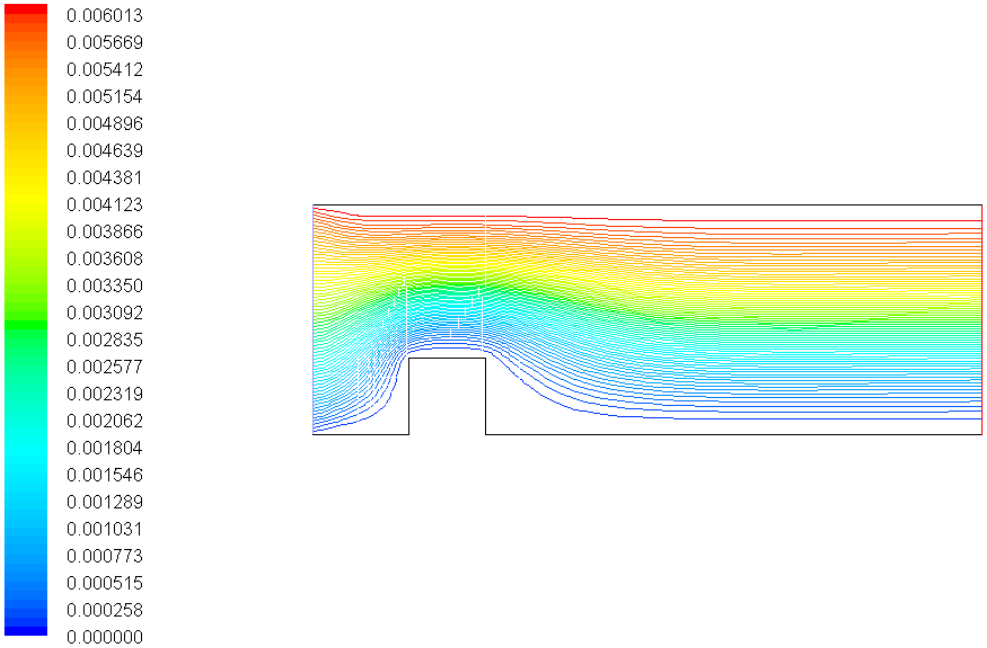


**Fig. 9 Stream function (Kg/s) ($R_e$ = 1)**

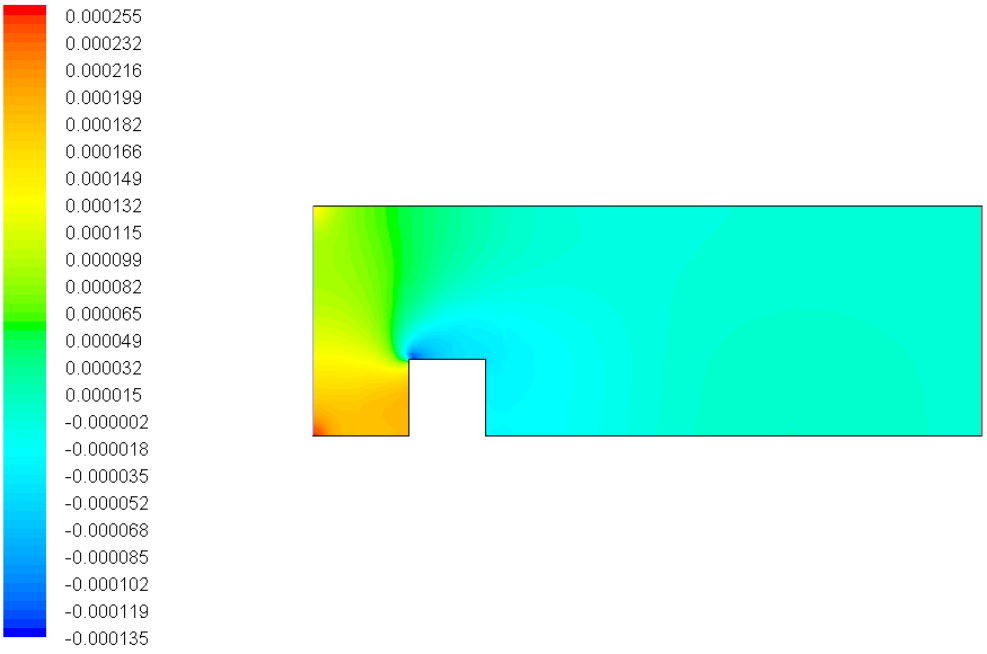


**Fig. 10 Static pressure ($R_e$ = 10)**

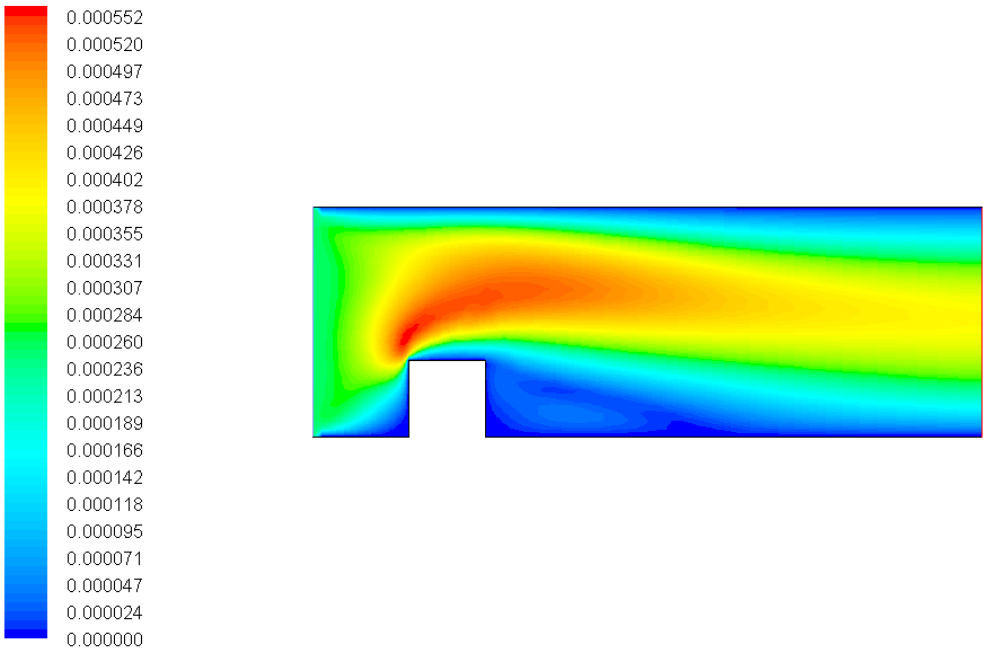


**Fig. 11 Velocity ($R_e$ = 10)**

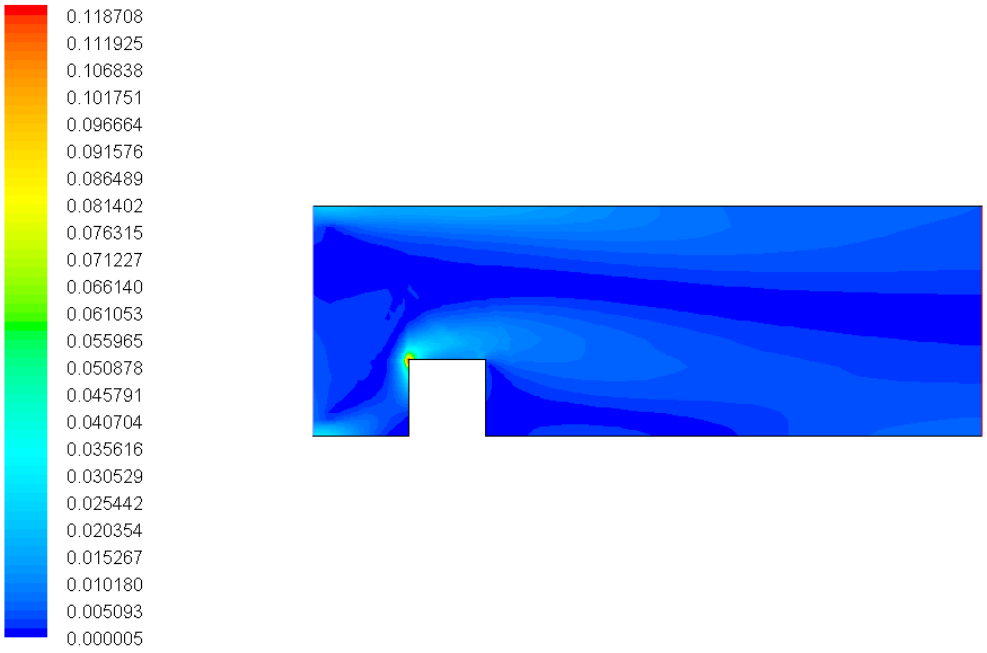


**Fig. 12 Vorticity magnitude (1/s) ($R_e$ = 10)**

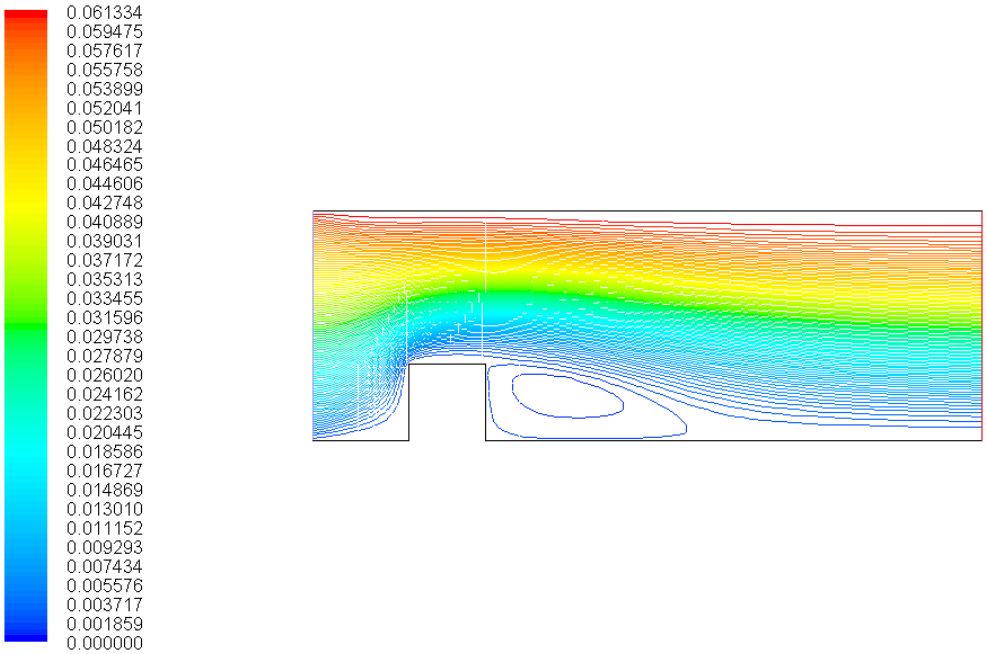


**Fig. 13 Stream function (Kg/s) ($R_e$ = 10)**

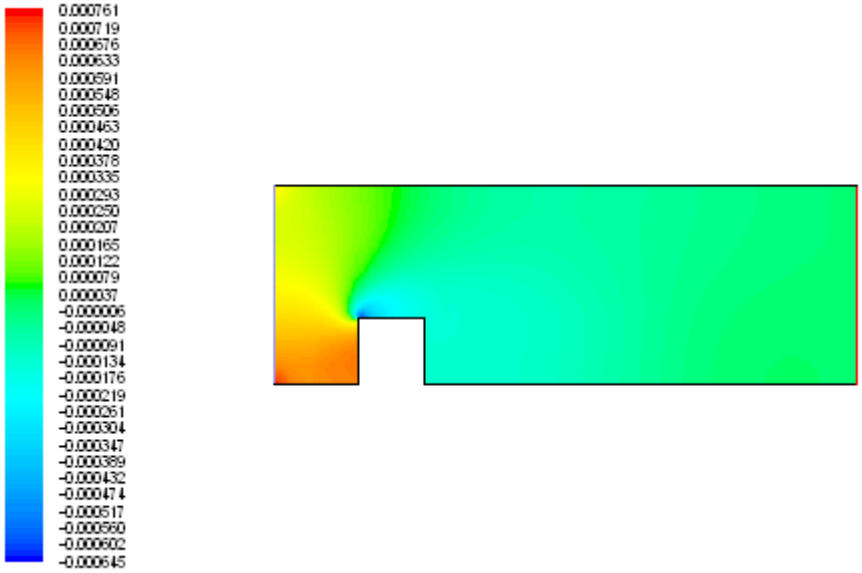


**Fig. 14 Static pressure ($R_e$ = 20)**

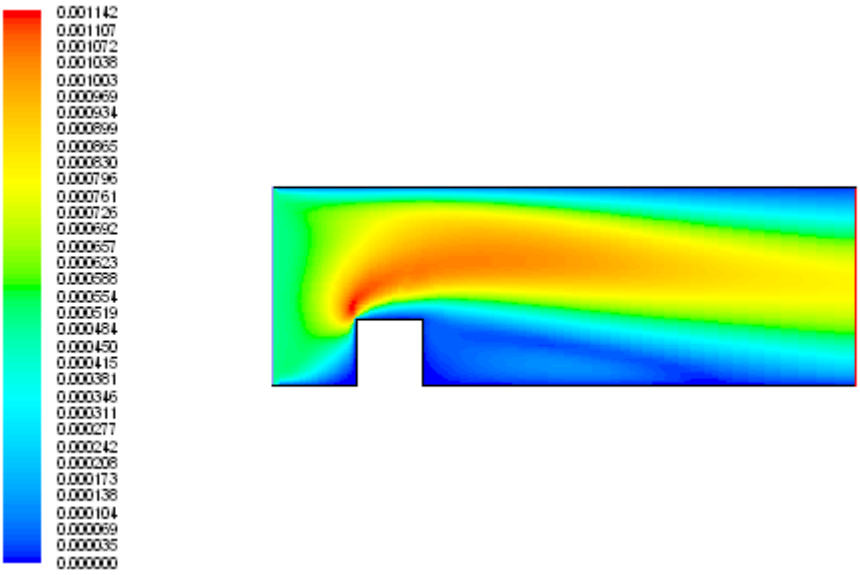


Fig. 15 Velocity ($R_e$ = 20)

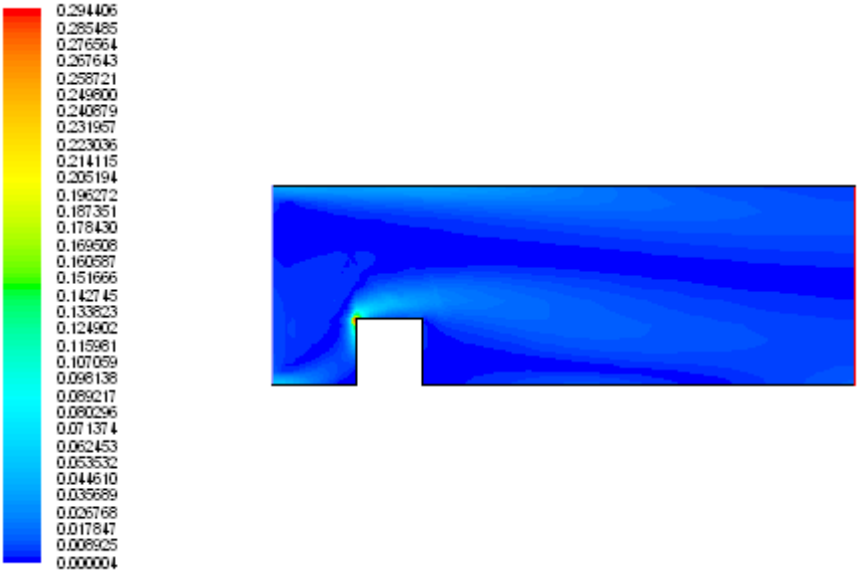


**Fig. 16 Vorticity magnitude (1/s) ($R_e$ = 20)**

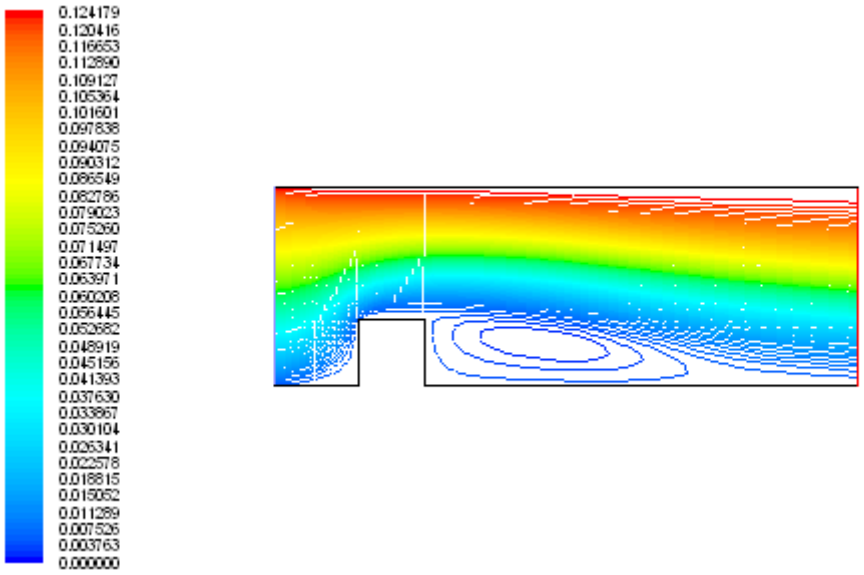


**Fig. 17 Stream function (Kg/s) ($R_e$ = 20)**

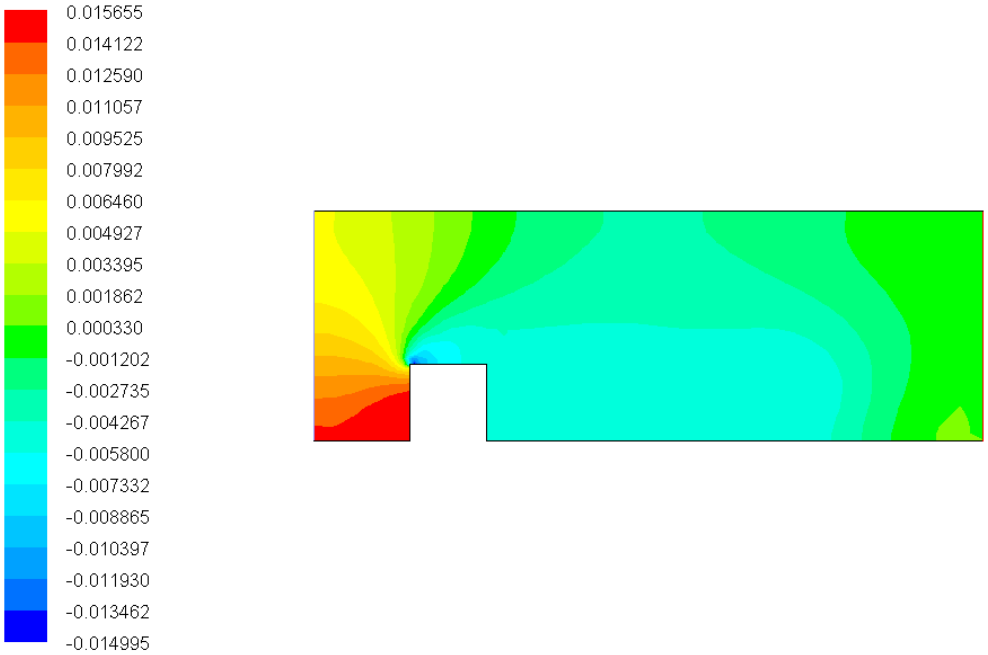


**Fig. 18 Static pressure ($R_e$ = 100)**

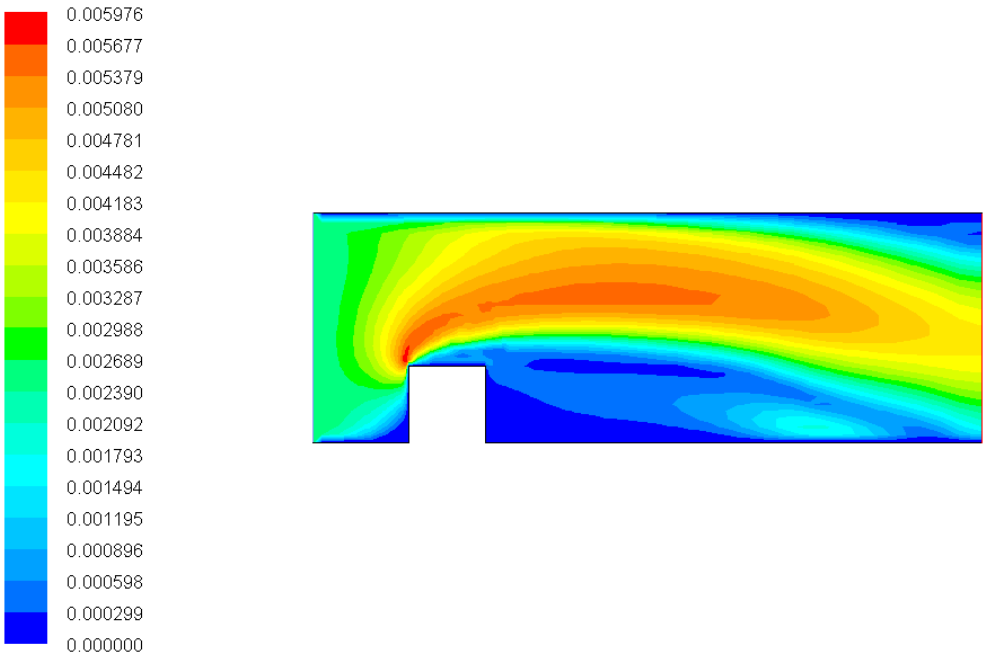


**Fig. 19 Velocity ($R_e$ = 100)**


**Fig. 20 Vorticity magnitude (1/s) ($R_e$ = 100)**

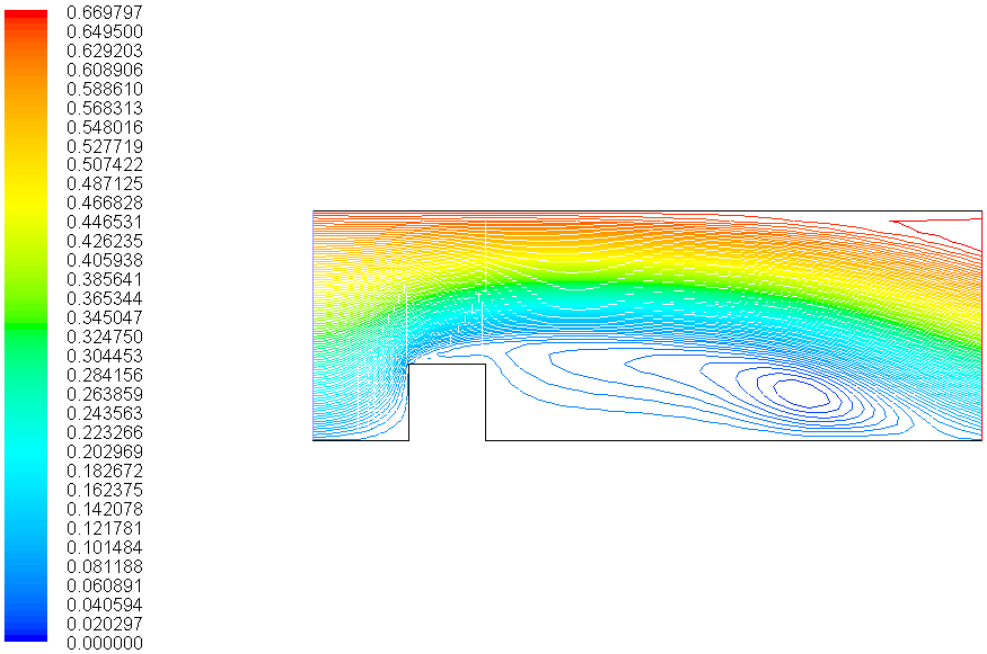


**Fig. 21 Stream function (Kg/s) ($R_e$ = 100)**

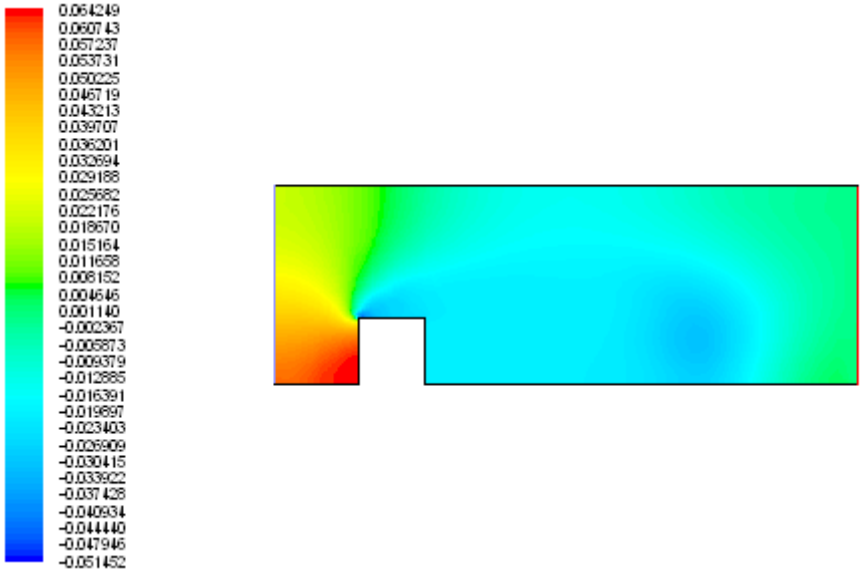


**Fig. 22 Static pressure ($R_e$ = 200)**

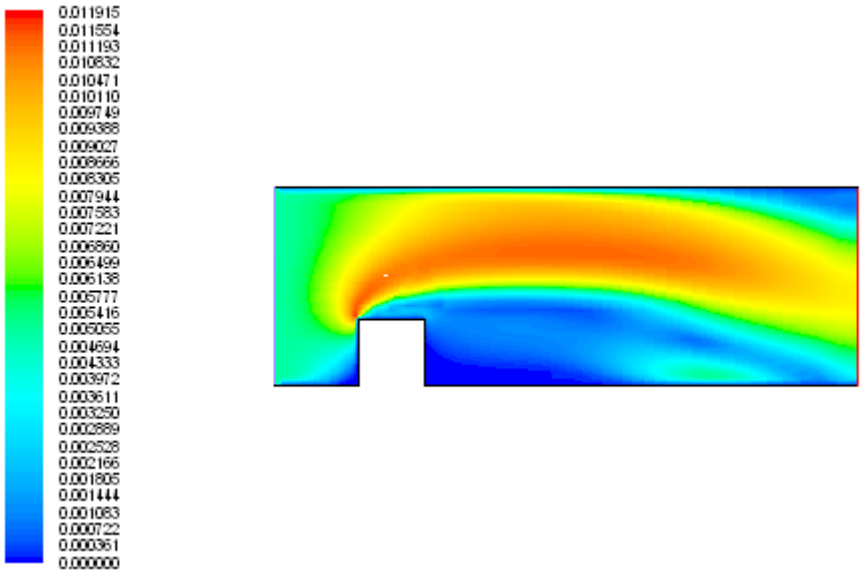


**Fig. 23 Velocity ($R_e$ = 200)**

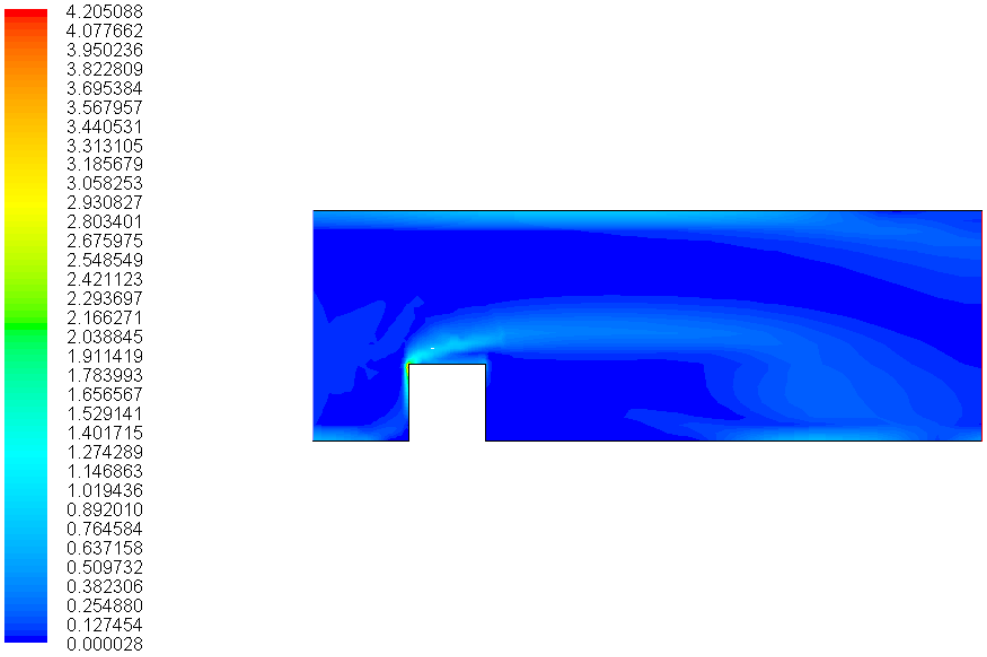


**Fig. 24 Vorticity magnitude (1/s) ($R_e$ = 200)**

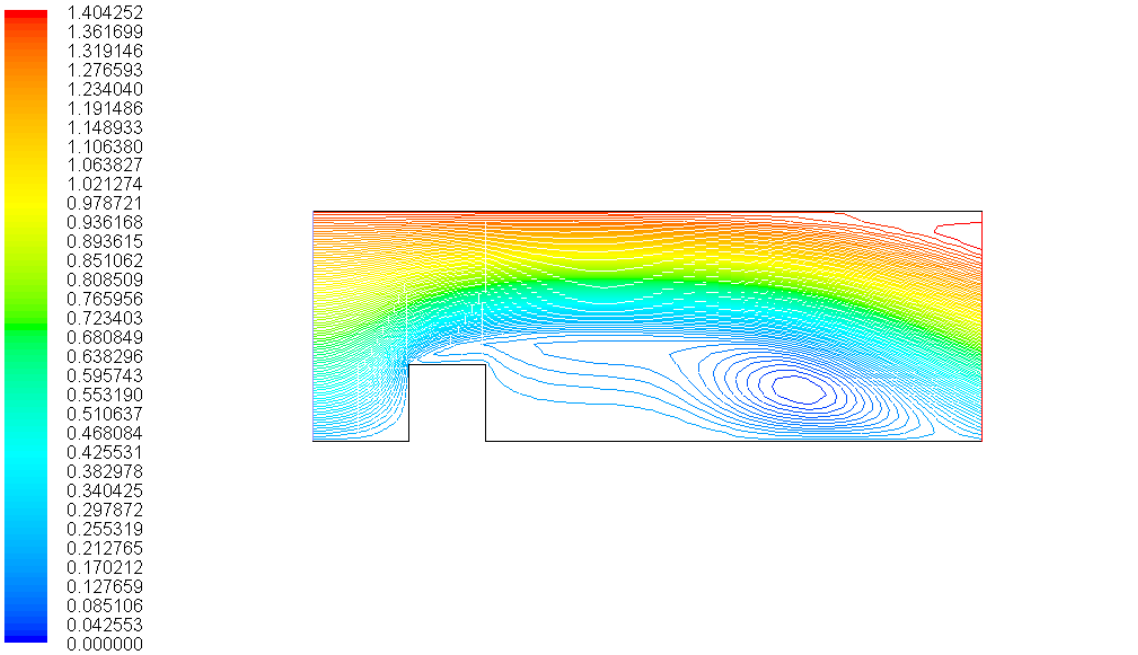


**Fig. 25 Stream function (Kg/s) ($R_e$ = 200)**

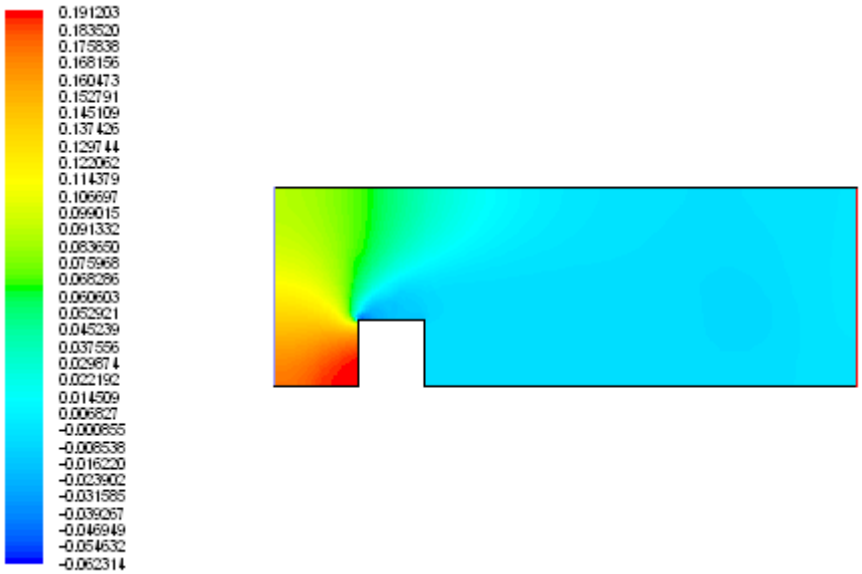


**Fig. 26 Static pressure ($R_e$ = 300)**

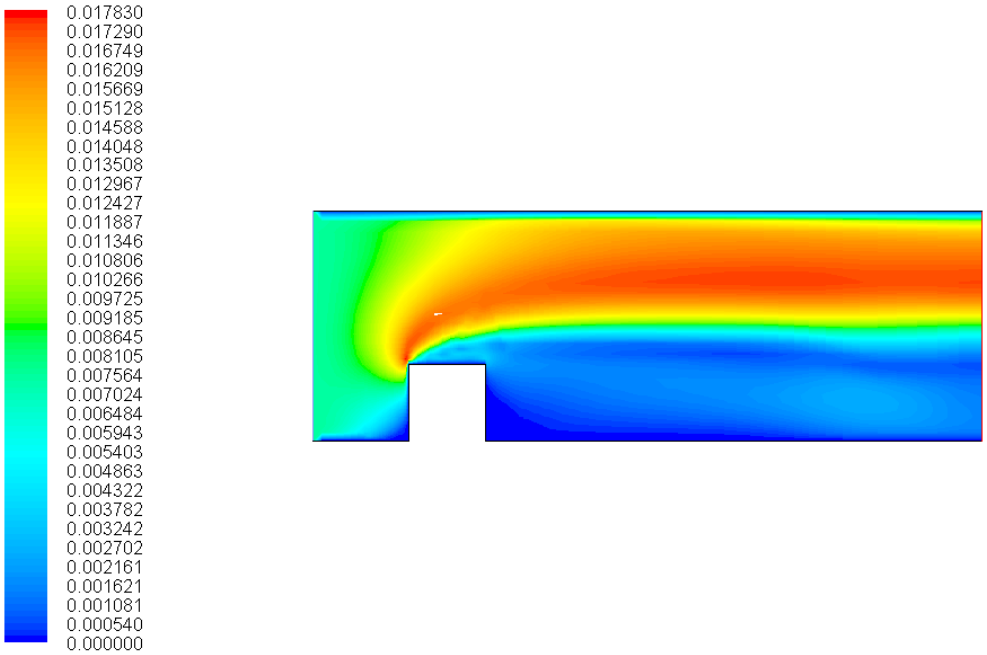


**Fig. 27 Velocity ($R_e$ = 300)**

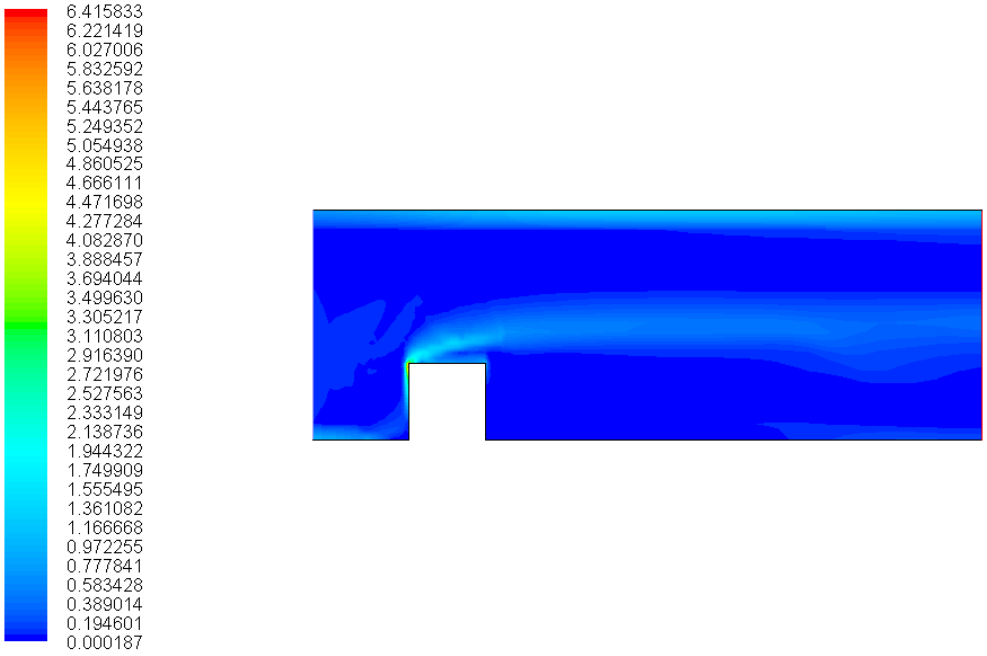


**Fig. 28 Vorticity magnitude (1/s) ($R_e$ = 300)**

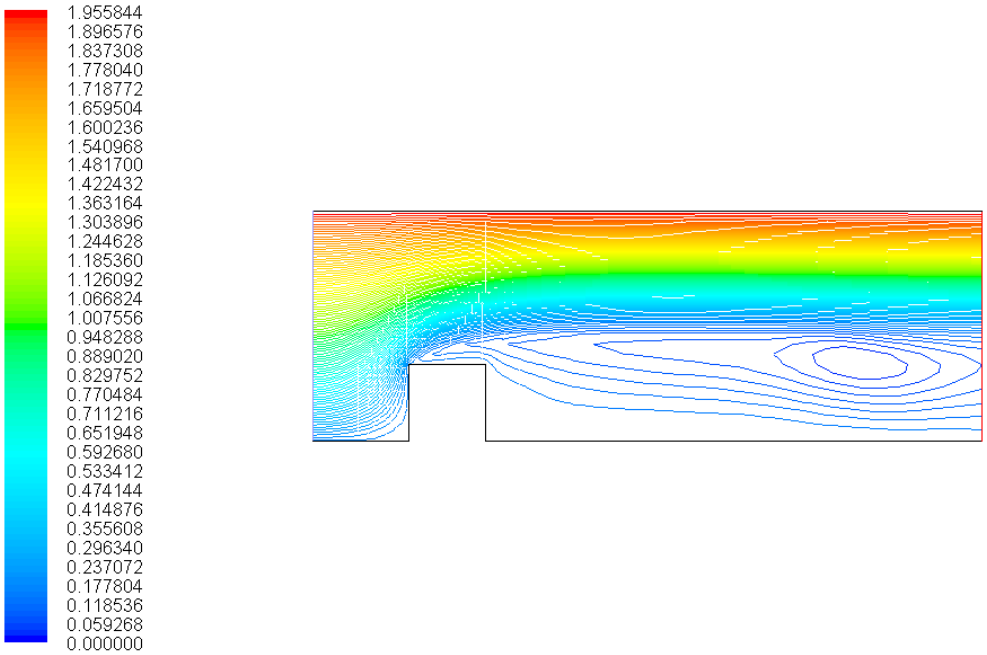


**Figure-29 Stream function (Kg/s) ($R_e$ = 300)**